Nonlinearity and Asymmetry of ENSO*

SOON-IL AN

International Pacific Research Center, SOEST, University of Hawaii at Manoa, Honolulu, Hawaii

FEI-FEI JIN

Department of Meteorology, SOEST, University of Hawaii at Manoa, Honolulu, Hawaii

(Manuscript received 13 June 2003, in final form 6 November 2003)

ABSTRACT

El Niño events (warm) are often stronger than La Niña events (cold). This asymmetry is an intrinsic nonlinear characteristic of the El Niño–Southern Oscillation (ENSO) phenomenon. In order to measure the nonlinearity of ENSO, the maximum potential intensity (MPI) index and the nonlinear dynamic heating (NDH) of ENSO are proposed as qualitative and quantitative measures. The 1997/98 El Niño that was recorded as the strongest event in the past century and another strong El Niño event in 1982/83 nearly reached the MPI. During these superwarming events, the normal climatological conditions of the ocean and atmosphere were collapsed completely. The huge bursts of ENSO activity manifested in these events are attributable to the nonlinear dynamic processes.

Through a heat budget analysis of the ocean mixed layer it is found that throughout much of the ENSO episodes of 1982/83 and 1997/98, the NDH strengthened these warm events and weakened subsequent La Niña events. This led to the warm–cold asymmetry. It is also found that the eastward-propagating feature in these two El Niño events provided a favorable phase relationship between temperature and current that resulted in the strong nonlinear dynamical warming. For the westward-propagating El Niño events prior to the late 1970s (e.g., 1957/58 and 1972/73 ENSOs) the phase relationships between zonal temperature gradient and current and between the surface and subsurface temperature anomalies are unfavorable for nonlinear dynamic heating, and thereby the ENSO events are not strong.

1. Introduction

The El Niño–Southern Oscillation (ENSO) is one of the most remarkable climate phenomena and has global climatic, ecological, and social impacts (Cane 1983; Philander 1983; Rasmusson and Wallace 1983). Great progress has been made in understanding and predicting ENSO (Cane and Zebiak 1985; Cane et al. 1986; Zebiak and Cane 1987; Schopf and Suarez 1988; Battisti and Hirst 1989; Philander 1990; Jin and Neelin 1993; Neelin et al. 1994, 1998). Theories based on the linear dynamics of the coupled ocean–atmospheric models have provided an understanding of the mechanisms for its oscillatory nature and its periodicity of about 3–5 yr. Small perturbations to the tropical climate system may grow into either El Niño or La Niña through the Bjerknes positive dynamic feedback of the ocean–atmosphere interaction in the equatorial Pacific. The equatorial SST zonal gradient drives the easterlies over the tropical Pacific and these easterlies in turn create the cold SST over the eastern Pacific resulting in the strengthening of the SST gradient (Bjerknes 1969). The transition from an El Niño to a La Niña event, and vice versa, is through a delayed negative feedback of ocean dynamical adjustment (Cane and Zebiak 1985; Wyrtki 1985; Cane et al. 1986; Zebiak and Cane 1987; Schopf and Suarez 1988; Battisti and Hirst 1989; Philander 1990; Jin and Neelin 1993; Neelin et al. 1994; Jin 1996, 1997; Neelin et al. 1998; An and Kang 2000; An and Jin 2001). The equatorial ocean heat content is slowly draining out (building up) during a warm (cold) ENSO phase as a result of the dynamic mass exchange between the equatorial belt and off-equatorial regions, leading to a phase reversal (Jin 1996, 1997).

The mechanism of the aforementioned positive and delayed negative feedbacks so far best represents the basic features of the ENSO-like oscillation. It also describes the coupled positive feedback for the growth of SST anomalies over the central to eastern Pacific and the transition due to subsurface ocean wave dynamics.

* School of Ocean and Earth Science and Technology Contribution Number 6323 and International Pacific Research Center Contribution Number 256.

Corresponding author address: Dr. Soon-Il An, International Pacific Research Center, SOEST, University of Hawaii at Manoa, Honolulu, HI 96822.
E-mail: sian@hawaii.edu

In conceptual models such as the delayed oscillator model (Suarez and Schopf 1988; Schopf and Suarez 1988; Battisti and Hirst 1989) and the recharge oscillator model (Jin 1996, 1997), ENSO is portrayed as a regular and periodic oscillatory behavior over the various parameter ranges. The observed characteristics of ENSO, however, are irregular and quasi-periodic. In addition to this behavior, the warm and cold events tend to occur most frequently during the boreal winter and the warm event is often stronger than the cold event.

The irregularity of ENSO and its phase locking with the annual cycle may be attributed to either nonlinear dynamics or stochastic forcing (Jin et al. 1994; Tziperman et al. 1994; Chang et al. 1994; Thompson and Battisti 2000). Jin et al. (1994) showed that including the seasonal cycle in a coupled model with ENSO oscillation and no atmosphere noise caused the frequency locking of various ENSO models to a constant period of 2 or 5 yr. The irregularity of warm- and cold-event recurrence could be explained by the devil's staircase scenario. Similar results were obtained by Tziperman et al. (1994) using a version of Suarez and Schopf's (1988) delayed oscillator model. An alternate hypothesis is that the ENSO was governed by a linear system with external stochastic forcing (Penland and Sardeshmukh 1995; Chang et al. 1996; Moore and Kleeman 1999; Thompson and Battisti 2000). For example, Thompson and Battisti (2000), using a linearized version of the Zebiak–Cane (ZC) ocean–atmosphere coupled model of ENSO (Zebiak and Cane 1987), showed that the growth of singular vectors had a strong tendency to peak in the boreal winter. They suggested that the annual cycle in the basic state of the ocean is sufficient to produce strong phase locking of ENSO to an annual cycle without invoking either nonlinearity or an annual cycle in the structure of the noise. Some statistical methods were also used to identify the nonlinearity and asymmetry of ENSO (Monahan 2001; Hannachi et al. 2003).

So far, however, the aforementioned arguments are not applied to the problem regarding the asymmetry between the warm and cold events. Theoretically the linear system cannot induce this asymmetry, even if the external stochastic forcing is involved. The traditional principal component analysis (a.k.a., empirical orthogonal function analysis) is a linear method that cannot identify the asymmetric feature between El Niño and La Niña except in the amplitude of the associated expansion coefficients, while the nonlinear principal component analysis, which detects low-dimensional nonlinear structure in multivariate datasets, characterizes the asymmetric spatial pattern between El Niño and La Niña (Monahan 2001). The ZC model (Cane and Zebiak 1985) that utilizes a strong nonlinear effect in the subsurface temperature parameterization produces a strong asymmetry between the warm and cold events. Without nonlinearity, the ZC model fails to produce asymmetry between warm and cold events (not shown here). In other words, the nonlinear dynamics may explain the unique asymmetry between the warm and cold events of ENSO.

Recently, Timmermann et al. (2003) proposed a nonlinear bursting scenario for extreme ENSO events. Jin et al. (2003) showed that the nonlinear dynamical thermal advections could play important roles in the apparent asymmetry between amplitudes of El Niño and La Niña events. Wang and McPhaden (2000) showed that the linear and nonlinear zonal advections were equally important in the eastern Pacific on the interannual time scale. In addition to the nonlinear dynamical advection there are several nonlinear processes in the tropical air–sea coupled system that may cause the asymmetric behavior of ENSO. These include the vertical mixing process in the ocean mixed layer that is more effective during the El Niño; oceanic tropical instability waves in the equatorial eastern Pacific, which are more active during the La Niña than El Niño (Wang and McPhaden 2000; Vialard et al. 2001); biological–physical feedback, which provides additional subsurface warming during the La Niña (Timmermann and Jin 2002); and the atmospheric nonlinear process such as the asymmetric response of the atmosphere to warm and cold SST anomalies (Kang and Kug 2002) and the thermodynamic control on deep convection (Hoerling et al. 1997). The nonlinear processes in the tropical coupled ocean–atmospheric system thus need to be investigated to determine what controls the strength of ENSO and why some El Niño events such as the 1982/83 and 1997/98 episodes attained such great intensities. A number of related issues—the reason for the warm–cold asymmetry in ENSO and how it is related to the concurring warming trend in the tropical Pacific in recent decades—remain unresolved.

This paper is an extension of Jin et al. (2003). In section 2, we discuss the measure of nonlinearity. Section 3 presents nonlinear dynamic processes that turn out to be critical for generating major El Niño events and responsible for the warm–cold asymmetry of ENSO. Section 4 shows why strong El Niños occurred during recent decades. Summary and discussion are given in section 5.

2. Measure of nonlinearity of ENSO

During the intense 1982/83 and 1997/98 El Niño events, peak warm anomalies of SST over the cold tongue region were as much as 5°C. The associated cold SST anomalies of the La Niña events had consistently smaller amplitude, about 2°–3°C. The great intensity of these ENSO cycles and their warm–cold asymmetry makes them ideal examples for examining nonlinearity in ENSO. Here we discuss some qualitative and quantitative measure of the nonlinearity of ENSO using the available observation datasets.

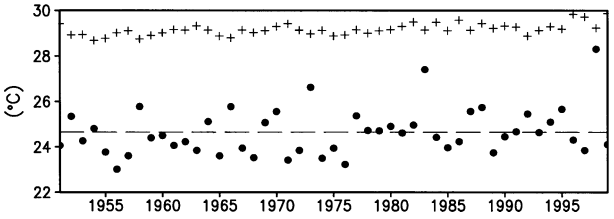

FIG. 1. Time series of winter mean (Dec–Feb) SST in the warm pool (+; averaged over the area 5°N–5°S, 130°–160°E) and in the cold tongue (●; averaged over the area 5°N–5°S, 120°–90°W).

a. Maximum potential intensity

El Niño (La Niña) refers to the abnormal warming (cooling) over the equatorial eastern Pacific—the so-called cold tongue region. One question that immediately comes to mind is how much can the cold tongue temperature be cooler or warmer. In other words, what are the upper and lower bounds of the cold tongue temperature? Here we define the upper and lower bounds as the maximum potential intensity (MPI) of ENSO as a theoretical measure.

As shown in Fig. 1, the cold tongue temperature during the El Niño almost reaches the climatologic warm pool temperature. The warm pool temperature is bounded by the radiative–convective equilibrium temperature (Waliser and Graham 1993) of about 30°C, which can be the upper bound of the equatorial eastern Pacific SST and thus the MPI of El Niño events. Similarly, the lower bound of the equatorial SST in the eastern Pacific, the MPI for La Niña events is about 20°C and corresponds to a complete surface outcropping of the thermocline. Thus, the cold tongue SST is bounded between 20°C and 30°C. Because the average SST in the cold tongue region is about 25°C, the MPI of ENSO measured by SST anomalies averaged in the cold tongue region is about 5°C.

One of the best examples of El Niño events that reach the MPI is the 1997/98 El Niño. The 1997/98 El Niño has been recorded as the strongest El Niño event ever instrumentally observed (McPhaden 1999). As shown in Fig. 2, the warm pool expanded so far to the east that the climatologic cold tongue vanished and the temperature during the 1997/98 winter (December 1997–

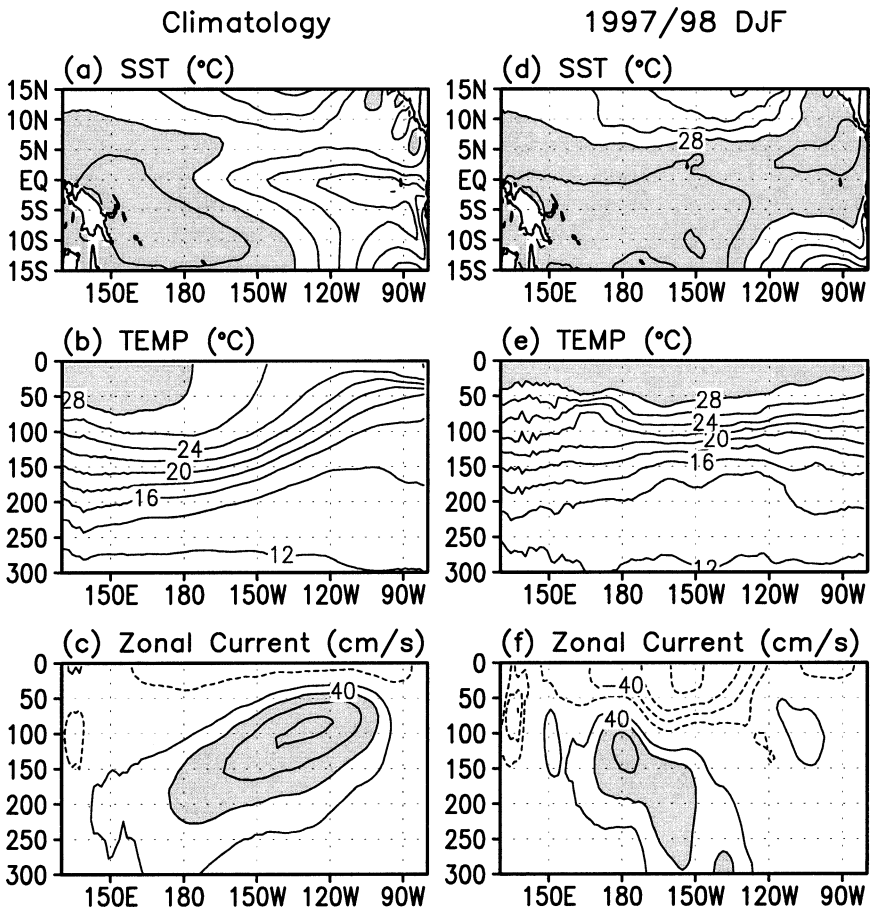

FIG. 2. (a) SST (°C), (b) upper-ocean temperature (°C), and (c) zonal current (cm s^{-1}) averaged for 20-yr winters (Dec–Feb); (d), (e), (f) are the same as in (a), (b), (c) except for the 1997/98 winter.

February 1998) reached more than 28°C, but climatologically was about 25°C. In addition, the climatological tilt of the thermocline (representing the sharp vertical temperature gradient region that separates the warm upper ocean from the cold abyssal deep ocean and approximating to the 20°C isotherm; Fig. 2c), in a dynamical quasi-equilibrium with the equatorial trade wind (Jin 1996; Yu and McPhaden 1999), was reversed (Fig. 2d). Even the equatorial undercurrent (Fig. 2c), a rather persistent ocean current, was significantly disrupted (Fig. 2d). Thus, anomalies in SST, thermocline, and ocean currents were too large to be possibly viewed as small perturbations to the normal tropical climate state. In other words, the normal climate state of the ocean and atmosphere completely collapsed during the mature phase of this 1997/98 El Niño event. Another strong El Niño event in 1982/83 that almost reached the MPI (see Fig. 1) bears a resemblance to the 1997/98 El Niño (not shown here). The nonlinear dynamic process might play an important role in establishing such huge deviations from the climate state.

The definition of MPI for ENSO is based on the current climate state of the tropical Pacific. The paleoclimate state of the tropical Pacific could be quite different. For a relatively cold tropical Pacific, such as during the glacial (cool) periods, the range of MPI could be less than the present MPI and the ENSO intensity might be lower (Tudhope et al. 2001). On the contrary, in a warmer climate such as one simulated under a global warming scenario, the MPI may further increase to allow strong ENSO activity (Timmermann et al. 1999).

b. Nonlinear dynamical heating

The fact that the strong 1982/83 and 1997/98 events reached the MPI for El Niño gives one measure of the ENSO nonlinearity. Another possible measure for the ENSO nonlinearity is the dominance of the nonlinear dynamical heating (NDH) in the heat budget of the upper ocean. The heat budget of the ocean surface layer can be obtained by using the following SST equation:

$$\frac{\partial T'}{\partial t} = -(u'\partial x\overline{T} + v'\partial y\overline{T} + w'\partial z\overline{T} + \overline{u}\partial xT' + \overline{v}\partial yT' + \overline{w}\partial zT') - (u'\partial xT' + v'\partial yT' + w'\partial zT') + R', \quad (1)$$

where T, u, v, w are SST, zonal, meridional, and vertical velocities, respectively. The overbar and prime denote the climatologic mean and anomalies, respectively. Surface heat flux and subgrid-scale contributions (e.g., small oceanic diffusion, heat flux due to tropical instability wave) are attributed to the residual term R. The second bracket of Eq. (1) indicates NDH. In section 3, we will show the observed NDH. Prior to examining the observed features, however we explore the role of NDH in a simple context.

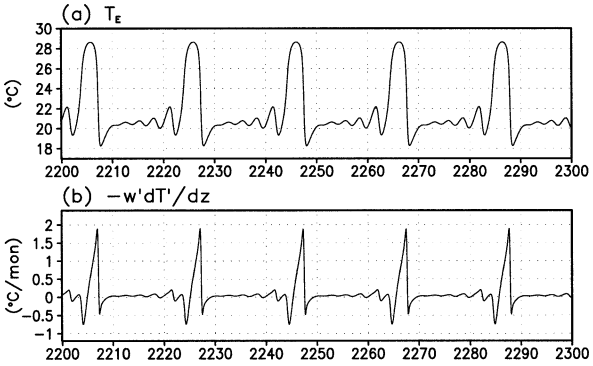

FIG. 3. (a) Time series of the SST (°C) in the eastern tropical Pacific obtained from the low-order nonlinear ENSO model (see the appendix). (b) Same as in (a) except for the SST tendency (°C month^{-1}) due to the anomalous vertical temperature advection by the anomalous upwelling ($-w'dT'/dz$).

In order to discuss the relationship between the strong El Niño and NDH, we first utilize the low-order ENSO model, which is the same prototype ENSO model that was used in Jin (1996, 1998) and Timmermann et al. (2003); the formulation is introduced in the appendix. The nonlinear effects in this low-order ENSO model are operated by the zonal and vertical dynamic advection terms in the SST equation [Eqs. (A1) and (A2), respectively]. The low-order nonlinear ENSO model produces the warm–cold asymmetric characteristics measured in the eastern Pacific SST (Fig. 3a), and also decadal occurrences of strong El Niño (warm) events, the so-called bursting behavior (Timmermann et al. 2003), in a broad model parameter range. The strong warm events are accompanied by a strong warming tendency due to NDH. During the weak minor event, NDH is weaker (Fig. 3b). The cooling tendency due to NDH is much weaker than the warming tendency due to NDH (Fig. 3b) so the strong cold events are not expected. Consequently, this low-order nonlinear ENSO model suggests that the NDH concurs with the El Niño (warm event) bursting, which also ultimately generates the strong El Niño–La Niña asymmetry.

Traditionally the nonlinear process was considered to limit the linear growth of the coupled system due to linear instability. The dominant nonlinearity in the Cane–Zebiak-type model (Zebiak and Cane 1987; Battisti 1988) is in the thermocline feedback. A very shallow or deep thermocline will stop further cooling or warming because of the nonlinear dependence of the SST on the thermocline depth in subsurface temperature parameterization (see the appendix). As an approximation of this tangent hyperbolic function, a symbolic cubic nonlinearity is often used to crudely represent nonlinearity in theoretical studies (e.g., Battisti and Hirst 1989; Jin 1997; Wang 2001). However, the cube term is an odd function, which yields symmetric warm–cold events. This nonlinear effect is only valid in the neighborhood of the climatological state that a model has

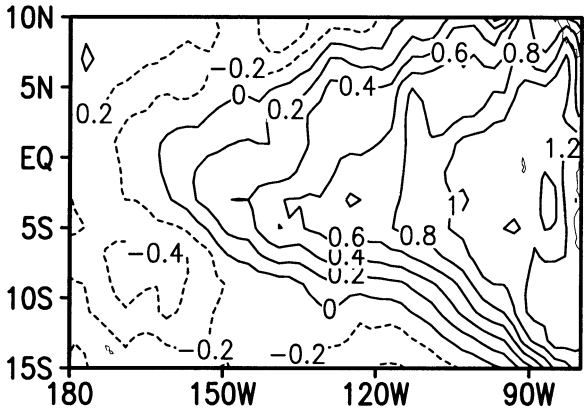

FIG. 4. Distribution of the skewness of tropical Pacific SST for the recent 50 yr.

been linearized onto (Jin 1997). The nonlinear advection, however, is not symmetric and thus the warm–cold asymmetry does occur even in the simple box model (Timmermann et al. 2003). Thus, NDH can be a useful measure of the nonlinearity of ENSO.

c. Statistical measure (skewness)

MPI and NDH are dynamical measures of the ENSO nonlinearity. Statistically, skewness can be another measure of the ENSO nonlinearity (Burgers and Stephenson 1999). This is because skewness is a measure of the asymmetry of a probability distribution function and is 0 for a normal distribution (White 1980). The moment coefficient of skewness is defined as the normalized third statistical moment,

$$\text{skewness} = \frac{m_3}{(m_2)^{3/2}}, \tag{2}$$

where m_k is the kth moment,

$$m_k = \sum_{i=1}^{N} \frac{(x_i - \overline{X})^k}{N},$$

and where x_i is the ith observation, $\overline{X}$ the mean, and N the number of observations. The statistical significance of skewness can be estimated from the standard error of skewness (White 1980) if the number of independent samples in an analyzed variable is known. The total number of warm (El Niño) and cold (La Niña) events in the equatorial eastern Pacific since 1950 is about 21 (Larkin and Harrison 2002), which may be a good estimation for a number of independent samples. Thus, according to White, the threshold for significant skewness at the 95% confidence level is about ± 1.0.

Figure 4 shows the skewness of SST anomalies over the tropical Pacific Ocean. The SST data are obtained from the National Centers for Environmental Prediction (NCEP) reconstructed monthly mean SST data (Reynolds and Smith 1994), which cover the period from 1950 to 2000. These data were constructed by applying the optimal reanalysis method, in which marine surface observations and the satellite Advanced Very High Resolution Radiometer (AVHRR) data were used. The anomalies are calculated by removing the climatological mean. There is a strong positive skewness over the central to eastern Pacific and weak negative skewness over the subtropical western Pacific. A similar skewness pattern was also found in the long-term simulation of the coupled general circulation model (Timmermann 1999). The skewness distribution appears to be directly related to the ENSO pattern. It indicates that the warm SST anomaly in the equatorial Pacific tends to be stronger than the cold SST anomaly. Likewise, El Niño is stronger than La Niña.

3. Role of the nonlinear dynamical heating

To evaluate the role of NDH, we calculated the heat budget in the layer of the uppermost 50 m of the tropical Pacific. To calculate each heat flux, NCEP ocean assimilation data (Ji et al. 1995; Behringer et al. 1998; Vossepoel and Behringer 2000) are used. NCEP ocean assimilation data consist of monthly mean ocean temperature, horizontal current, salinity, wind stress, and sea level pressure. The vertical velocity is calculated using the horizontal currents under the continuity assumption. The horizontal resolution is $1^\circ \times 1.5^\circ$ and vertical resolution is 10 m in the upper 100-m depth. The NCEP data cover January 1980–January 2000. Observed surface and subsurface ocean temperatures as well as satellite altimetry sea level data from TOPEX/Poseidon were assimilated into a Pacific basin ocean general circulation model (OGCM). The OGCM was forced with weekly surface winds and heat fluxes of NCEP operational atmospheric analyses. Recently, the first version of NCEP ocean assimilation system has been modified. Behringer et al. (1998) described a new version of the NCEP ocean assimilation data that incorporates a number of modifications to the ocean assimilation system described by Ji et al. (1995). As an example of improvement over the old version, they showed that the surface currents in this new version were closer to the estimation from surface drifter data for 1978–94 that was reported by Acero-Schertzer et al. (1997), and Vossepoel and Behringer (2000), who also showed that the assimilation of TOPEX/Poseidon observations improved dynamics height simulation without degrading the temperature. NCEP data had been also used for assimilation in initializing ENSO prediction models, by which their prediction skill was improved (Tang et al. 2003). However, some shortcomings in the old version remain in the new version. The surface heat flux forcing is the climatological mean annual cycle; there is no freshwater flux, instead, the model's surface salinity field was relaxed to the climatological annual cycle. Thus, the warming trend due to the enhanced greenhouse gases is not actively engaged, and the long-term tropical climate changes that might be related to the

salinity field (e.g., Schneider 2000) are not reflected in these data.

NCEP data are too short to investigate the long-term changes. The simple ocean data assimilation (SODA) set (Carton et al. 2000) was used. SODA data were built by interpolating unevenly distributed ocean measurements into three-dimensional global fields of temperature, salinity, and current velocity using an ocean general circulation model. SODA data consist of the same variables as NCEP data, but the vertical resolution is about 15 m in the upper ocean and its period is from January 1950 to December 2001. The Tropical Ocean Global Atmosphere/Tropical Atmosphere Ocean array (TOGA/TAO) data and TOPEX/Poseidon data are used for checking the quality of the SODA dataset (e.g., Carton et al. 2000; Xie et al. 2002). The zonal, meridional, and ocean temperature at each layer from the surface (7.5 m) to a depth of 52.5 m are utilized.

The heat budget of the uppermost 50 m of the ocean surface layer is calculated using Eq. (1). In this calculation, for the NCEP (SODA) data the mixed layer depth is fixed at 50 m (45 m) depth, which includes five (three) vertical layers. Wang and McPhaden (2000), on the contrary, performed the heat budget analysis for a varying mixed layer. They defined the mixed layer depth at which the temperature is 0.5°C lower than the sea surface temperature. Following their definition of the mixed layer, we also calculate NDH for varying mixed layer depth. The result turns out to be very similar to the NDH for the fixed mixed layer depth (not shown here), indicating that the budget analysis is quite robust.

Figure 5 shows the nonlinear advective heating rate averaged for the 1997/98 El Niño (July 1997/May 1998), 1998/99 La Niña (July 1998/May 1999), 1986/87 El Niño (October 1986/August 1987), and 1988/89 La Niña (July 1988/May 1989). For the 1986/87 El Niño, we select a slightly different season from others because the SST anomaly during this event matured during the spring of 1987. As shown in Fig. 5, the warming tendency due to the NDH that centered at the equatorial central to eastern Pacific commonly appeared during either El Niño or La Niña, so it served to amplify the El Niño event but to weaken the following La Niña event. During the 1997/98 El Niño the NDH reached 2°C month^{-1} over the central-eastern equatorial Pacific. Nearly the same amount of NDH also appeared during the following 1998/99 La Niña event, while during the 1986/87 El Niño and the 1988/89 La Niña the NDH was negligible. In other words, the strong (weak) ENSO events are associated with the strong (weak) positive NDH.

The time evolutions of the SST tendency over the region of 5°N–5°S and 170°–100°W due to linear and nonlinear advective heating are shown in Fig. 6. For each time series, a 3-month running average has been applied. As shown in Fig. 6, the nonlinear heating is as strong as the linear advective heating throughout much of the ENSO episodes of 1982/83 and 1997/98. The amplitudes of these strong ENSO events were strongly skewed toward the warm event. On the contrary, during the modest and weak ENSO events such as 1986/87, the nonlinear advective heat was negligible and the warm and cold SST anomalies had similar amplitudes. This suggests that the intensity and asymmetric behavior of strong ENSO events can be attributable to NDH.

The evolution features of each nonlinear advective heating along the equator (1°N–1°S) are shown in Fig. 7. The 11-month running average has been applied to each term. As shown in the figure, the vertical advective heating is strongest among the nonlinear dynamical heating, and the zonal advective heating is the second strongest. The meridional advective heating is negligible. The peaks of the NDH (e.g., nonlinear vertical advective heating) appear during the developing and decaying phases of El Niño, and there is a local minimum of NDH between two peaks, which matches the El Niño peak time (e.g., 1997/98 and 1982/83 winters). It is obvious that SST anomaly reaches its peak value when the SST tendency is 0. Thus, this local minimum of SST tendency due to NDH indicates that the seasonal phase locking of El Niño is also attributable to NDH.

In this budget analysis, we could not resolve the dynamical heating due to the tropical instability waves (TIW) using the monthly mean data so that the heat flux due to TIW had not been included in this budget analysis. The dynamical heating due to TIW is stronger during the La Niña, and it almost disappears during the El Niño (Philander 1990). This is because the variability of TIW is nearly proportional to the meridional temperature/momentum gradient near the eastern equatorial Pacific. It is known that the heat flux due to TIW plays an important role of the mean heat balance in the equatorial eastern Pacific (Vialard et al. 2001). Throughout the El Niño (from March 1997 to May 1998), the SST tendency over the equatorial eastern Pacific due to TIW is negative (~0.5°C month^{-1}), acting as a negative feedback to the growth of El Niño (Vialard et al. 2001), which is opposite to NDH obtained from the monthly data.

4. Propagation characteristics and nonlinear dynamical heating

Previously, we showed that the NDH could cause a strong ENSO event as well as the asymmetric behavior of ENSO. Then, one may ask why a particular El Niño event has a strong asymmetric feature and why the strong ENSO event frequently occurred during the recent decades. In this section, we will show that the El Niño having the eastward-propagating feature is favorable for the strong NDH, and the strong ENSO during the recent decades commonly shows the eastward-propagating feature.

The temporal and spatial correlation between the temperature and current fields determines the intensity of NDH. If the temperature (or more precisely the tem-

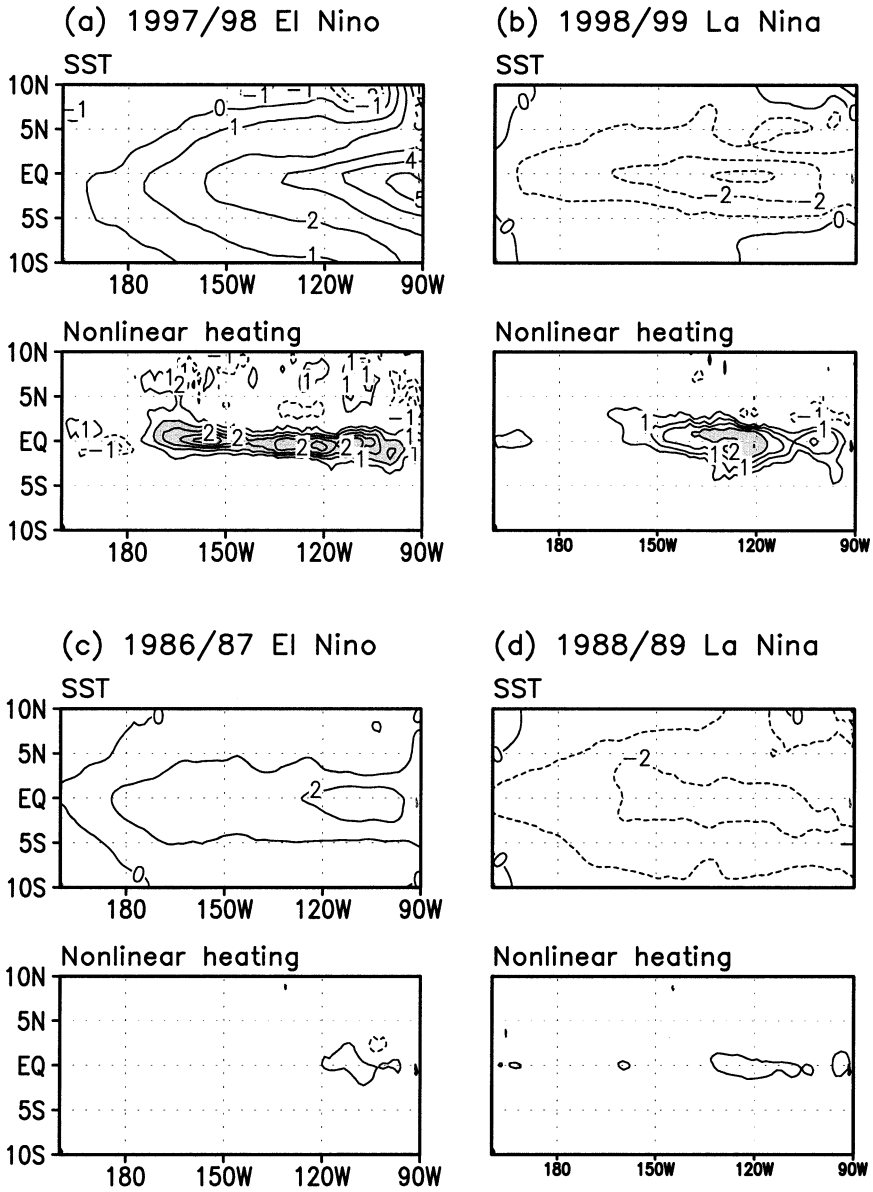

FIG. 5. SST anomaly (°C) and rate of change in SST (°C month^{-1}) due to the nonlinear dynamic heating during (a) the 1997/98 El Niño (Jul 1997–May 1998), (b) the 1998/99 La Niña (Jul 1998–May 1999), (c) the 1986/87 El Niño (Oct 1986–Aug 1987), and (d) the 1988/89 La Niña (Jul 1988–May 1989).

perature gradient) and current fields are both spatial and temporal in-phase so that they are highly correlated, the NDH becomes large. By examining the nonlinear vertical advection, which is the most dominant term of NDH (see Fig. 7), we can illustrate that NDH due to vertical advection is facilitated by certain temporal and spatial phase differences in the temperature gradient and current fields during the ENSO cycles. We will focus on the two strong El Niños that occurred since 1980 (1982/83 and 1997/98) and two moderate El Niños that occurred in 1957/58 and 1972/73. Because NCEP ocean assimilation data only cover the period after 1980, SODA data are used as an alternative. The NDH for the 1982/83 and 1997/98 El Niños calculated using SODA data is similar to that using NCEP data. This suggests that the results for SODA data may provide useful information about NDH before the 1980s.

First, we examined the 1982/83 El Niño [Jin et al. (2003) examined the 1997/98 episode]. In order to understand the intrinsic characteristics of NDH, we subdivide the nonlinear vertical advective heating so that the nonlinear vertical heating anomaly ($-w'dT'/dz$) was decomposed into the anomalous upwelling (w') and vertical temperature gradient (dT'/dz). The vertical tem-

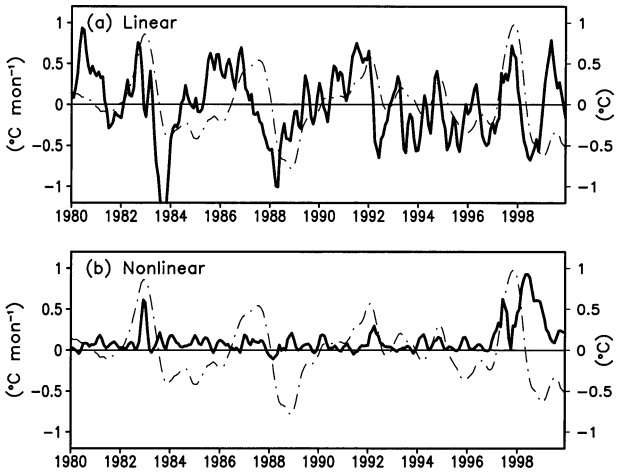

FIG. 6. Time series of SST tendencies (°C month^{-1}) (a) due to the linear dynamical heating, and (b) due to the nonlinear dynamical heating averaged over 5°N–5°S, 170°–100°W. The 3-month running mean has been used. The dashed–dot line in each panel indicates the SST anomaly (°C) averaged over the same region.

perature gradient separated into the SST and the subsurface temperature anomalies. The zonal wind stress anomalies were also shown, because the wind stress was considered to be the major force driving the upwelling and was directly linked to the SST anomalies. In Fig. 8 we showed the equatorial zonal wind stress, mixed layer SST, subsurface temperature at 65 m, upwelling at the surface layer depth (w'), vertical temperature gradient (dT'/dz) (defined as the difference between SST and subsurface temperature), and the nonlinear vertical advective heating anomalies ($-w'dT'/dz$). During the developing phase of El Niño (spring and summer of 1982), there were westerly wind stress anomalies in the central to western equatorial Pacific and easterly wind anomalies in the eastern Pacific. These anomalies in zonal wind stress are consistent with the linear atmospheric response to atmospheric forcing associated with the SST anomalies (Fig. 8c). The westerly (easterly) wind stress anomalies induced anomalous equatorial downwelling (upwelling) (Fig. 8b). The deepening of the thermocline depth in the eastern equatorial Pacific resulted in the adiabatic warming in the subsurface ocean (Fig. 8d), leading to warm SST anomalies (Fig. 8c). Thus, during the warm phase of El Niño the warm anomalies in the subsurface ocean were larger than the warm SST anomalies in the eastern equatorial Pacific (Fig. 8e). At the same time there was an enhanced upwelling due to the easterly wind anomalies in the eastern equatorial Pacific. This situation allowed a nonlinear enhancement of the vertical advection of the anomalous warm water in the subsurface to the surface layer and thus resulted in a nonlinear acceleration of the surface warming.

Similarly, from the transition to the La Niña phase,

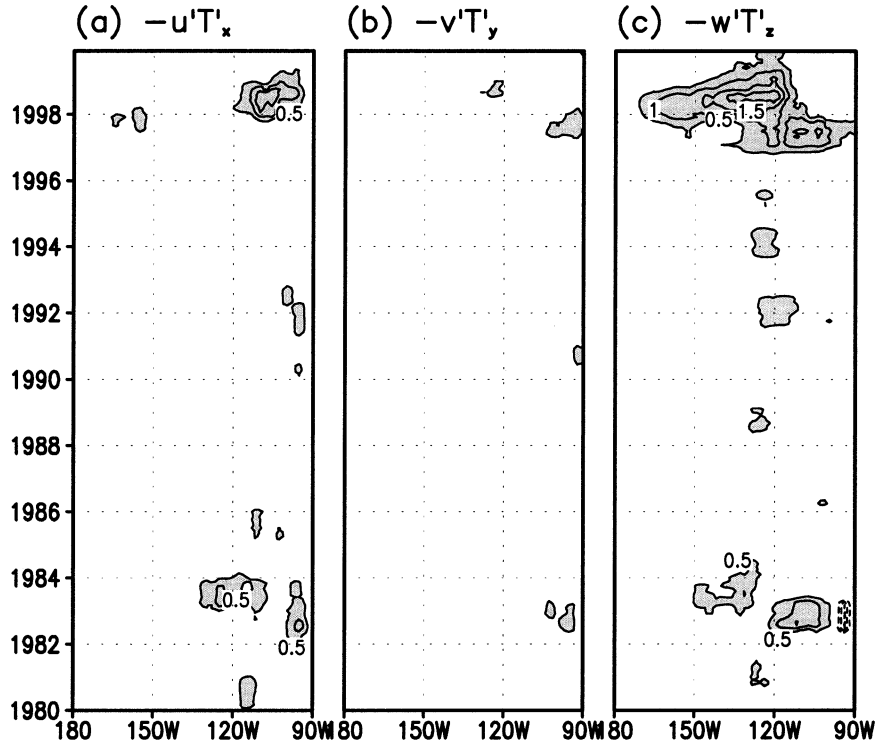

FIG. 7. Time–longitude cross section of the nonlinear dynamic heating rate (°C month^{-1}) due to (a) zonal advection, (b) meridional advection, and (c) vertical advection along the equator (1°N–1°S). The 11-month running mean has been used.

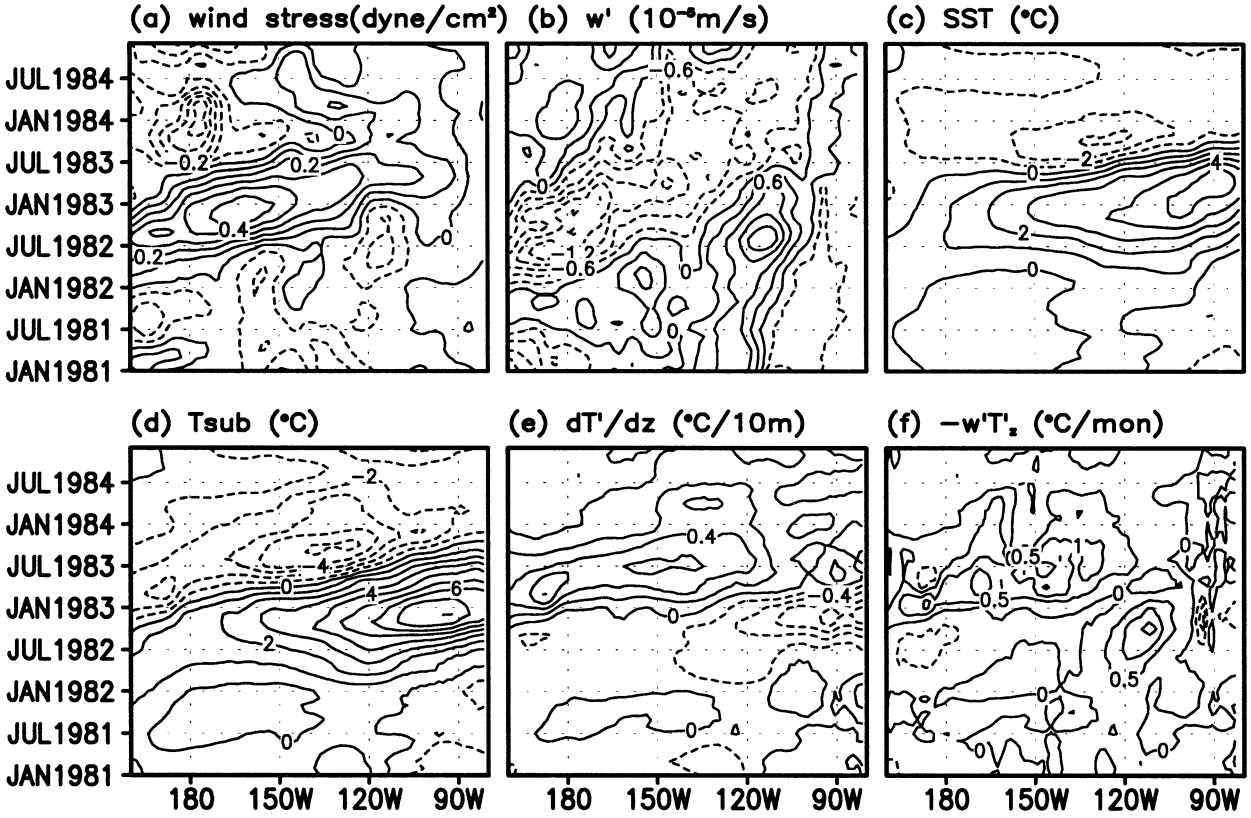

FIG. 8. (a) Wind stress (dyn cm^{-2}), (b) upwelling velocity (10^{-5} m s^{-1}), (c) ocean temperature anomaly in the surface layer (°C), (d) subsurface ocean temperature (obtained at 65-m depth; °C), (e) vertical temperature difference (between surface layer and the subsurface; (× 0.1°C m^{-1}), and (f) nonlinear vertical advective heating rate (°C $month^{-1}$) along the equator. Time series cover from Jan 1981 to Dec 1984.

anomalous cooling in the subsurface ocean is larger than that in the surface layer of ocean in the eastern Pacific. At the same time, there is an anomalous downwelling due to the westerly wind anomalies in the eastern equatorial Pacific. The penetration of the anomalous cold water from the subsurface to the surface layer is further reduced because of the reduced vertical temperature gradient. It again results in an anomalous nonlinear warming. Therefore, the out-of-phase relationship between the anomalies in the vertical temperature difference (surface and subsurface temperature) and the vertical upwelling velocity in the eastern equatorial Pacific gives rise to the nonlinear dynamic warming tendency through the ENSO cycle. This nonlinear warming strengthens the El Niño event and dampens the following La Niña event for the major ENSO episodes in 1982/83 and 1997/98.

The two major El Niño events in the past two decades had eastward propagation of the equatorial SST and zonal wind stress anomalies, while the El Niño events prior to the late 1970s had westward propagations (Rasmusson and Carpenter 1982; Wallace et al. 1998). This decadal change in the propagation characteristics of ENSO might be attributed to decadal changes in the tropical ocean–atmosphere climatological states (An and Jin 2000; Fedorov and Philander 2000; Wang and An 2001, 2002). As shown in Fig. 9, the SST and subsurface temperature anomalies during the 1982/83 and 1997/98 ENSO events propagate to the east, while those during the 1957/58 and 1972/73 ENSO events propagate to the west. For the 1982/83 and 1997/98 ENSO events, the strong vertical temperature gradient can be attributed to the phase difference between the SST and subsurface temperature via the eastward propagation. Its phase relationship with the strong upwelling causes the strong nonlinear dynamic warming. On the other hand, for the 1957/58 and 1972/73 ENSOs, the evolutions of SST are almost in-phase with that of subsurface temperature, resulting in the small vertical temperature gradient. In addition to this small vertical temperature gradient, the anomalous upwelling tends to be located to west of the center of the SST anomaly (An and Wang 2000) so the upwelling and the vertical temperature gradient are not in-phase. As the result, the nonlinear dynamic heating prior to 1980 was weaker. Therefore the propagation characteristics of ENSO are a useful indicator for anticipating potential nonlinear amplifications and thus intensities of ENSO events, which remain difficult to predict.

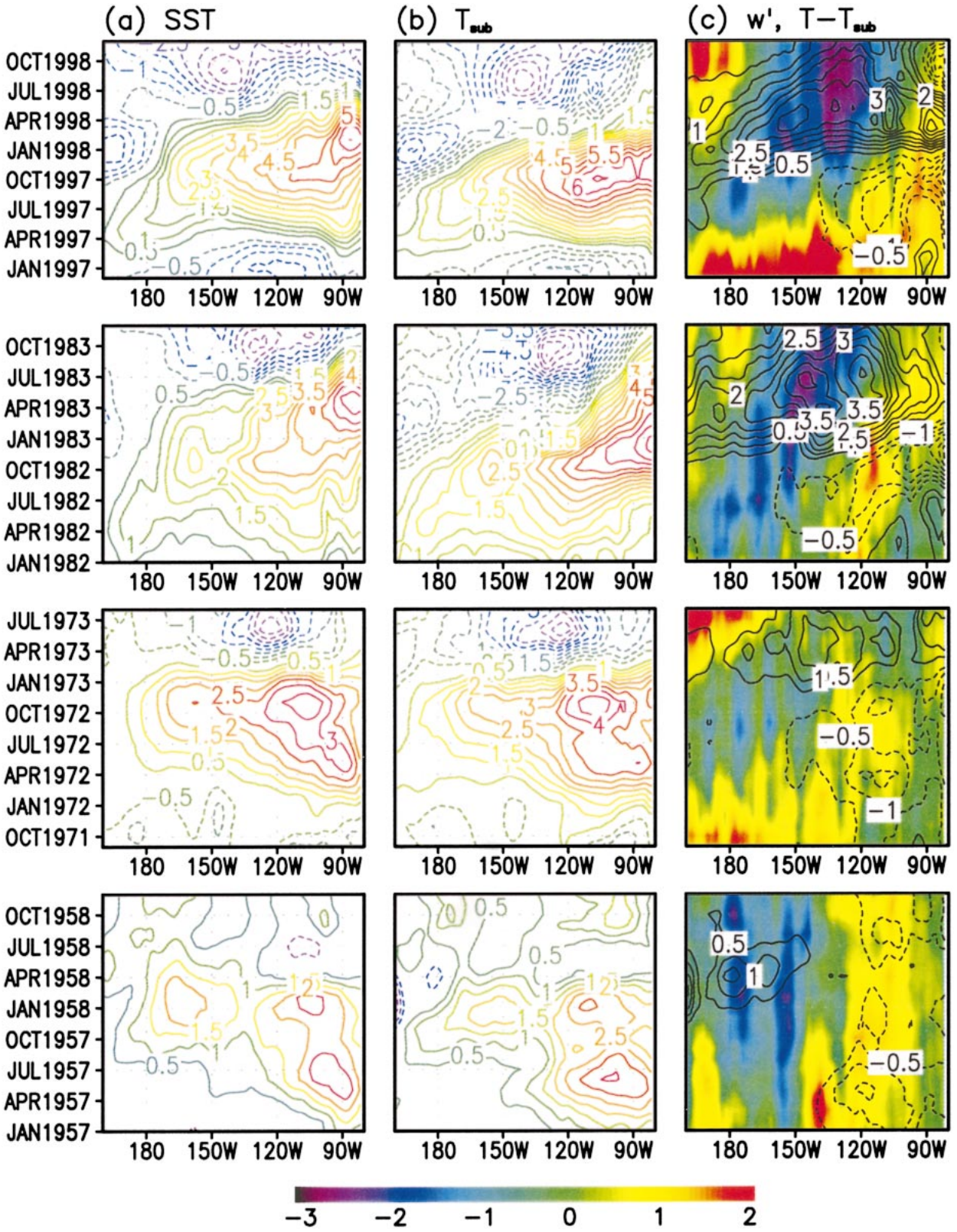

FIG. 9. (a) SST (°C), (b) subsurface ocean temperature (obtained at 65-m depth; °C), and (c) upwelling velocity (in color; $\times 10^{-5}$ m s^{-1}), vertical temperature difference between surface layer and the subsurface (in contour; °C). From the (bottom) to the (top): 1957/58, 1972/73, 1982/83, 1997/98 El Niños are shown.

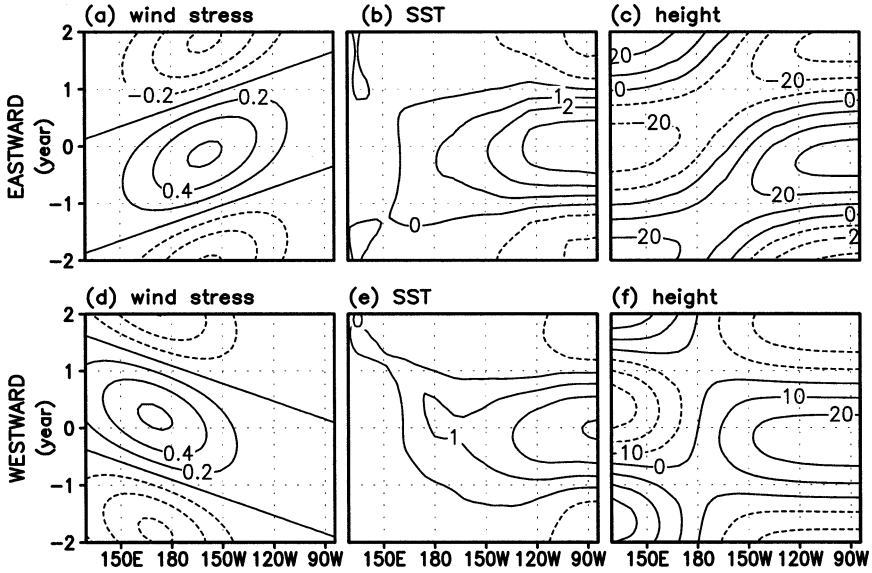

FIG. 10. (a) Wind stress (dyn cm^{-2}), (b) SST (°C), and (c) thermocline depth (m) obtained from the ocean dynamic model response to a given eastward-propagating wind forcing; (d), (e), (f) are the same as in (a), (b), (c), respectively, except for the westward-propagating wind forcing.

To investigate the dependence of NDH on the propagation characteristics of the coupled system, we examined the dynamical connection in the changes between the propagating direction and the nonlinear vertical advection. A reduced gravity ocean model is used to identify the consequences resulting from the changes of the propagating direction of the system. The ocean model is basically the same as that used in the Cane–Zebiak model (Zebiak and Cane 1987). We specify an anomalous wind stress as follows:

$$\tau_x(x, y, t) = 0.5 \sin[2\pi(\omega t - \lambda x)]\left[\Psi_0\left(\frac{y}{L_y}\right) - \Psi_2\left(\frac{y}{L_y}\right)\right] \times \left\{\exp\left[-\left(\frac{x - x_0}{L_x}\right)^2\right]\right\}, \quad (3)$$

where the horizontal structure is specified on the basis of the leading singular value decomposition (SVD) mode between zonal wind and SST anomalies (see Fig. 1 of Wang and An 2001). The functions ψ_0 and ψ_2 are the zeroth and the second Hermite functions, respectively. The longitudinal position of the maximum wind stress is specified by x_0 with L_x (=45° latitudinal length) and L_y (=9°) as the zonal and meridional *e*-folding scales, respectively. The frequency ω is set as ¼ yr^{-1} and λ is the control parameter of propagation speed of the wind patch.

We performed two experiments in which the prescribed wind patch was designed to propagate either eastward (''E run'') or westward (''W run''). For the E run we used $\lambda = 2/3$ and $x_0 = 160°$W, and for the W run $\lambda = -2/3$ and $x_0 = 170°$E. The evolution features of equatorial zonal wind stress, SST, and dynamic height anomalies (as a proxy of subsurface temperature anomalies) for one cycle are shown in Fig. 10. As shown in Fig. 10, when the wind forcing moves eastward (westward), SST anomalies also tend to move eastward (westward). As expected, the SST and height anomalies over the central-eastern Pacific in the W run are almost in phase in terms of time and space, indicating that the difference between surface and subsurface temperature is small over the whole period of ENSO. The phase difference between SST and height anomalies in the E run is larger over the central Pacific and somewhat less over the eastern Pacific. This difference is due to the eastward propagation of the wind patch as well as the oceanic response. When both the wind patch and SST anomaly propagate eastward, the resulting phase relationship favors the strong nonlinear advective heating (Figs. 8 and 9). For the westward-propagating events, the nonlinear advective heating becomes much weaker because the phase relationship between the surface temperature and the subsurface temperature becomes more in phase. These numerical experiments further suggest that eastward-propagating ENSO events may facilitate NDH and have the potential for being nonlinearly intensified.

5. Conclusions and discussion

The episodic bursting of the intense El Niño events in recent decades (1982/83 and 1997/98) was partly generated by nonlinear intensifications through the dynamical processes. These eastward-propagating ENSO events had the necessary temporal and spatial phase differences in temperature and current fields to facilitate the dynamic heating effect in the equatorial upper ocean

through nonlinear vertical and zonal advections. This nonlinear heating enhances the amplitude of the warm phase and reduces the amplitude of the cold phase of ENSO and thus results in the warm–cold asymmetry. This asymmetry has a nonlinear rectification effect on the climate mean state (Jin et al. 2003). In the past half century, ENSO characteristics have undergone some significant changes (An and Jin 2000; Urban et al. 2000; Wang and An 2001). The changes in ENSO have been also attributed to the changes in the climate background state, due to either interdecadal climate variability or global warming (Timmermann et al. 1999; An and Jin 2000; Fedorov and Philander 2000; Urban et al. 2000; Wang and An 2001, 2002). However, our evidence indicates that the changing ENSO is also responsible for this warming trend and changes in the climate background state in the tropical Pacific.

The state-of-the-art coupled ocean–atmosphere climate models for global warming simulations now have advanced to the point where it is possible to resolve the basic features of ENSO. Most coupled general circulation models (CGCMs) simulated enhanced eastern equatorial Pacific warming due to the greenhouse gas increase (Meehl and Washington 1996; Knutson and Manabe 1998; Roeckner et al. 1999; Jin et al. 2001). These results generally implied that the positive feedback due to a local dynamical enhancement effect on tropical warming could overwhelm the negative feedback due to a dynamic thermostat effect (Sun and Liu 1996; Cane et al. 1997; Noda et al. 1999) that was postulated to provide a regulating mechanism for the warm pool SST. Some recent studies of the ENSO response to increases in greenhouse gases using the coupled ocean–atmosphere models found an increase in the amplitude of ENSO (Timmermann 1999; Timmermann et al. 1999; Collins 2000), whereas some earlier studies found little or no changes in ENSO behavior as greenhouse gases increase (Tett 1995; Knutson et al. 1997). Urban et al. (2000) did an observational analysis that showed that the climate state change during the early 1920s and the late 1970s concurred with ENSO variability. On the contrary, Solow and Huppert (2003) argued that the nonstationarity of ENSO is not clear. Nevertheless, as shown here, not only the ENSO characteristics but also NDH has been markedly changed during the past several decades. The enhanced NDH in turn may reinforce the warming trend in the eastern tropical Pacific (Jin et al. 2003).

Our analysis of NDH provides only a rough indication of the importance of nonlinear dynamics in the tropical ocean–atmosphere interaction. However, a more careful, detailed examination of the nonlinear processes is needed. For instance, a highly nonlinear process is involved in the mixed layer dynamics of the upper ocean. In the upper ocean, vertical mixing is constrained by the stratification of the vertical mean temperature profile (Galanti et al. 2002). The stably stratified vertical temperature distribution (the strong vertical temperature gradient), which appeared during La Niña, obstructs the vertical mixing. During El Niño the temperature difference between the surface and subsurface decreases, which may allow more vertical mixing. Therefore, the role of mixed layer in the ENSO nonlinearity warrants further study. The tropical oceanic instability waves in the equatorial eastern Pacific are another source that may contribute to ENSO asymmetry through nonlinear process. The increase of the meridional temperature gradient and currents near the eastern equatorial Pacific during La Niña accompany more TIWs, which tend to mix warm off-equatorial water and cold equatorial water and prevent the equatorial cold tongue from cooling down. During El Niño the TIWs disappear (Philander 1990; Vialard et al. 2001). Thus, the heat flux due to the oceanic instability waves is nonlinear. Nonlinear process is also necessary to translate intraseasonal [a.k.a., Madden–Julian oscillation (MJO)] forcing into interannual signals. Kessler and Kleeman (2000) suggested that the MJO could interact constructively with the ENSO cycle through nonlinear rectification and that rectified SST anomalies caused the stronger El Niño. Further study of ENSO nonlinearity may deepen our understanding of ENSO asymmetry and extreme ENSO events.

Acknowledgments. This work was supported by National Science Foundation Grant ATM-0226141 and by National Oceanographic and Atmospheric Administration Grants GC01-229 and GC01- 246. Soon-Il An was supported by Frontier Research System for Global Change through its sponsorship of the International Pacific Research Center. The authors thank Shang-Ping Xie for the valuable comments, and Diane Henderson and May Izumi for the careful reading and editing of the manuscript.

APPENDIX

Low-Order Nonlinear ENSO Model

The model is derived from a simplified version of the Zebiak and Cane (1987) ENSO model using a two-strip and a two-box approximation (Jin 1998; Timmermann et al. 2003). The heat budget of the ocean surface layer can be expressed as follows:

$$\frac{dT_1}{dt} = -\alpha(T_1 - T_r) - \frac{u}{L/2}(T_2 - T_1), \quad \text{(A1)}$$

$$\frac{dT_2}{dt} = -\alpha(T_2 - T_r) - \frac{w}{H_m}(T_2 - T_{\text{sub}}), \quad \text{(A2)}$$

where T_1 and T_2 represent the eastern and western equatorial temperature, respectively; $1/\alpha$ a thermal damping time scale; T_{sub} is subsurface temperature; w is upwelling velocity; u is zonal velocity; and H_m and L are the depth of the mixed layer and the basin width, respectively. The first terms in both (A1) and (A2) indicate the thermal

relaxation process toward a radiative–convective equilibrium temperature T_r, and the second terms indicate the zonal and vertical temperature advection process, respectively. Equations (A3)–(A5) represent the wind stress related to the Walker circulation, the zonal current directly induced by the wind stress, and the equatorial upwelling due to the Ekman flow divergence:

$$\tau = -\mu(T_1 - T_2)/\beta, \tag{A3}$$

$$u/(L/2) = \varepsilon\beta\tau, \tag{A4}$$

$$w/H_m = -\zeta\beta\tau, \tag{A5}$$

where ε and ζ measure the strength of zonal and vertical advection, respectively, and μ is a coupling coefficient representing the coupling strength between air and sea. The subsurface temperature T_{sub} is parameterized as (Jin 1996)

$$T_{\text{sub}} = T_r - (T_r - T_{r0}) \times \{1 - \tanh[(H + h_2 - z_0)/h^*]\}/2, \tag{A6}$$

where T_{r0} is the temperature beneath the thermocline, h_2 is the depth departure of the eastern equatorial thermocline from its reference depth H, z_0 is the depth at which w takes its characteristic values, and h^* measures the sharpness of the thermocline.

Following the recharge oscillator formulation used in Jin (1997), the dynamical equations for the thermocline depth anomalies in the western (h_1) and eastern (h_2) equatorial Pacific are represented as follows:

$$\frac{dh_1}{dt} = -rh_1 - \left(\frac{rbL}{2}\right)\tau, \tag{A7}$$

$$h_2 = h_1 + bL\tau. \tag{A8}$$

A slow adjustment process due to the nonequilibrium adjustment of the tropical Pacific Ocean and a degenerated Sverdrup balance between the equatorial east–west thermocline depth and wind stress (An and Jin 2001) are adopted in (A7) and (A8), respectively. The parameter values used in this study are $T_{r0} = 16$°C, $T_r = 29.5$°C, $\alpha = 1/180$ day^{-1}, $r = 1/400$ day^{-1}, $H_m = 50$ m, $H = 100$ m, $z_0 = 75$ m, $h^* = 62$ m, $\mu = 0.0026$ K^{-1} day^{-1}, $\mu bL/\beta = 22$ m K^{-1}, $\zeta = 1.3$, $\varepsilon = 0.11$, and $L = 15 \times 10^6$ m.

REFERENCES

Acero-Schertzer, C. E., D. V. Hanse, and M. S. Swenson, 1997: Evaluation and diagnosis of surface currents in the National Centers for Environmental Prediction's ocean analyses. *J. Geophys. Res.*, **102,** 21 037–21 048.

An, S.-I., and F.-F. Jin, 2000: An eigen analysis of the interdecadal changes in the structure and frequency of ENSO mode. *Geophys. Res. Lett.*, **27,** 2573–2576.

——, and I.-S. Kang, 2000: A further investigation of the recharge oscillator paradigm for ENSO using a simple coupled model with zonal mean and eddy separated. *J. Climate,* **13,** 1987–1993.

——, and B. Wang, 2000: Interdecadal change of the structure of the ENSO mode and its impact on the ENSO frequency. *J. Climate,* **13,** 2044–2055.

——, and F.-F. Jin, 2001: Collective role of thermocline and zonal advective feedbacks in the ENSO mode. *J. Climate,* **14,** 3421–3432.

Battisti, D. S., 1988: The dynamics and thermodynamics of a warming event in a coupled tropical atmosphere–ocean model. *J. Atmos. Sci.,* **45,** 2889–2919.

——, and A. C. Hirst, 1989: Interannual variability in a tropical atmosphere–ocean model: Influence of the basic state, ocean geometry and nonlinearity. *J. Atmos. Sci.,* **46,** 1687–1712.

Behringer, D. W., M. Ji, and A. Leetmaa, 1998: An improved coupled model for ENSO prediction and implication for ocean initialization. Part I: The ocean data assimilation system. *Mon. Wea. Rev.,* **126,** 1013–1021.

Bjerknes, J., 1969: Atmospheric teleconnections from the equatorial Pacific. *Mon. Wea. Rev.,* **97,** 163–172.

Burgers, G., and D. B. Stephenson, 1999: The ''normality'' of El Niño. *Geophys. Res. Lett.,* **26,** 1027–1030.

Cane, M. A., 1983: Oceanographic events during El Niño. *Science,* **222,** 1189–1195.

——, and S. E. Zebiak, 1985: A theory of El Niño and the Southern Oscillation. *Science,* **228,** 1084–1087.

——, ——, and S. C. Dolan, 1986: Experimental forecasts of El Niño. *Nature,* **321,** 827–832.

——, A. C. Clement, A. Kaplan, Y. Kushnir, D. Pozdnyakov, R. Seager, S. E. Zebiak, and R. Murtugudde, 1997: Twentieth-century sea surface temperature trends. *Science,* **275,** 957–960.

Carton, J., G. Chepurin, X. Cao, and B. Giese, 2000: A simple ocean data assimilation analysis of the global upper ocean 1950–95. Part I: Methodology. *J. Phys. Oceanogr.,* **30,** 294–309.

Chang, P., B. Wang, T. Li, and L. Ji, 1994: Interactions between seasonal cycle and the Southern Oscillation: Frequency entrainment and chaos in an intermediate coupled ocean–atmosphere model. *Geophys. Res. Lett.,* **21,** 2817–2820.

——, L. Ji, H. Li, and M. Flugel, 1996: Chaotic dynamic versus stochastic process in ENSO in coupled ocean–atmosphere models. *Physica D,* **9,** 301–320.

Collins, M., 2000: The El Niño–Southern Oscillation in the second Hadley Centre coupled model and its response to greenhouse warming. *J. Climate,* **13,** 1299–1312.

Fedorov, A. V., and S. G. Philander, 2000: Is El Niño changing? *Science,* **288,** 1997–2002.

Galanti, E., E. Tziperman, M. Harrison, A. Rosati, R. Giering, and Z. Sirkes, 2002: The equatorial thermocline outcropping—A seasonal control on the tropical Pacific ocean–atmosphere instability strength. *J. Climate,* **15,** 2721–2739.

Hannachi, A., D. Stephenson, and K. Sperber, 2003: Probability-based methods for quantifying nonlinearity in the ENSO. *Climate Dyn.,* **20,** 241–256.

Hoerling, M. P., A. Kumar, and M. Zhong, 1997: El Niño, La Niña, and the nonlinearity of their teleconnections. *J. Climate,* **10,** 1769–1786.

Ji, M., A. Leetmaa, and J. Derber, 1995: An ocean analysis system for seasonal to interannual climate studies. *Mon. Wea. Rev.,* **123,** 460–481.

Jin, F.-F., 1996: Tropical ocean–atmosphere interaction, the Pacific cold tongue, and the El Niño–Southern Oscillation. *Science,* **274,** 76–78.

——, 1997: An equatorial ocean recharge paradigm for ENSO. Part I: Conceptual model. *J. Atmos. Sci.,* **54,** 811–829.

——, 1998: A simple model for Pacific cold tongue and ENSO. *J. Atmos. Sci.,* **55,** 2458–2469.

——, and J. D. Neelin, 1993: Modes of interannual tropical ocean–atmosphere interaction—A unified view. Part I: Numerical results. *J. Atmos. Sci.,* **50,** 3477–3502.

——, ——, and M. Ghil, 1994: El Niño on the devil's staircase: Annual subharmonic steps to chaos. *Science,* **264,** 70–72.

——, Z.-Z. Hu, M. Latif, L. Bengtsson, and E. Roeckner, 2001:

Dynamical and cloud-radiation feedbacks in El Niño and greenhouse warming. *Geophys. Res. Lett.,* **28,** 1539–1542.
——, S.-I. An, A. Timmermann, and J. Zhao, 2003: Strong El Niño events and nonlinear dynamical heating. *Geophys. Res. Lett.,* **30,** 1120, doi:10.1029/2002GL016356.
Kang, I.-S., and J.-S. Kug, 2002: El Niño and La Niña sea surface temperature anomalies: Asymmetric characteristics associated with their wind stress anomalies. *J. Geophys. Res.,* **107** (D19), 4372–4381.
Kessler, W. S., and R. Kleeman, 2000: Rectification of the Madden–Julian oscillation into the ENSO cycle. *J. Climate,* **13,** 3560–3575.
Knutson, T. C., and S. Manabe, 1998: Model assessment of decadal variability and trends in the tropical Pacific. *J. Climate,* **11,** 2273–2296.
——, ——, and D. Gu, 1997: Simulated ENSO in a global coupled ocean–atmosphere model: Multidecadal amplitude modulation and CO_2 sensitivity. *J. Climate,* **10,** 138–161.
Larkin, N. K., and D. E. Harrison, 2002: ENSO warm (El Niño) and cold (La Niña) event life cycles: Ocean surface anomaly patterns, their symmetries, asymmetries, and implications. *J. Climate,* **15,** 1118–1140.
McPhaden, M. J., 1999: The child prodigy of 1997–1998. *Nature,* **398,** 559–562.
Meehl, G. A., and W. M. Washington, 1996: El Niño-like climate change in a model with increased CO_2 concentrations. *Nature,* **382,** 56–60.
Monahan, A. H., 2001: Nonlinear principal component analysis: Tropical Indo-Pacific sea surface temperature and sea level pressure. *J. Climate,* **14,** 219–233.
Moore, A. M., and R. Kleeman, 1999: Stochastic forcing of ENSO by the intraseasonal oscillation. *J. Climate,* **12,** 1199–1220.
Neelin, J. D., M. Latif, and F.-F. Jin, 1994: Dynamics of coupled ocean–atmosphere models: The tropical problem. *Annu. Rev. Fluid Mech.,* **26,** 617–659.
——, D. Battisti, A. Hirst, F.-F. Jin, Y. Wakata, T. Yamagata, and S. Zebiak, 1998: ENSO theory. *J. Geophys. Res.,* **103,** 14 262–14 290.
Noda, A., K. Yamaguchi, S. Yamaki, and S. Yukimoto, 1999: Relationship between natural variability and CO_2-induced warming pattern: MRI AOGCM experiment. Preprints, *10th Symp. on Global Change Studies,* Dallas, TX, Amer. Meteor. Soc., 359–362.
Penland, C., and P. D. Sardeshmuhk, 1995: The optimal growth of tropical sea surface temperature anomalies. *J. Climate,* **8,** 1999–2004.
Philander, S. G. H., 1983: El Niño Southern Oscillation phenomena. *Nature,* **302,** 295–301.
——, 1990: *El Niño, La Niña, and the Southern Oscillation.* Academic Press, 293 pp.
Rasmusson, E. M., and T. H. Carpenter, 1982: Variations in tropical sea surface temperature and surface wind fields associated with the Southern Oscillation/El Niño. *Mon. Wea. Rev.,* **110,** 354–384.
——, and J. M. Wallace, 1983: Meteorological aspects of the El Ninõ/Southern Oscillation. *Science,* **222,** 1195–1202.
Reynolds, R. W., and T. M. Smith, 1994: Improved global sea surface temperature analysis using optimum interpolation. *J. Climate,* **7,** 929–948.
Roeckner, E., L. Bengtsson, J. Feichter, L. Lelieveld, and H. Rodhe, 1999: Transient climate change simulations with a coupled atmosphere–ocean GCM including the tropospheric sulfur cycle. *J. Climate,* **12,** 3004–3032.
Schneider, N., 2000: A decadal spiciness mode in the Tropics. *Geophys. Res. Lett.,* **27,** 257–260.
Schopf, P. S., and M. J. Suarez, 1988: Vacillations in a coupled ocean–atmosphere model. *J. Atmos. Sci.,* **45,** 549–566.
Solow, A. R., and A. Huppert, 2003: On non-stationarity of ENSO. *Geophys. Res. Lett.,* **30,** 1910, doi:10.1029/2003GL018225.
Suarez, M. J., and P. S. Schopf, 1988: A delayed action oscillator for ENSO. *J. Atmos. Sci.,* **45,** 3283–3287.
Sun, D., and Z. Liu, 1996: Dynamic ocean–atmosphere coupling: A thermostat for the Tropics. *Science,* **272,** 1148–1150.
Tang, T., R. Kleeman, A. M. Moore, A. Weaver, and J. Vialard, 2003: The use of ocean reanalysis products to initialize ENSO predictions. *Geophys. Res. Lett.,* **30,** 1694, doi:10.1029/2003GL017664.
Tett, S. F. B., 1995: Simulation of El Niño–Southern Oscillation–like variability in a global AOGCM and its response to CO_2 increase. *J. Climate,* **8,** 1473–1502.
Thompson, C. J., and D. S. Battisti, 2000: A linear stochastic dynamical model of ENSO. Part I: Model development. *J. Climate,* **13,** 2818–2832.
Timmermann, A., 1999: Detecting the nonstationary response of ENSO to greenhouse warming. *J. Atmos. Sci.,* **56,** 2313–2325.
——, and F.-F. Jin, 2002: Phytoplankton influences on tropical climate. *Geophys. Res. Lett.,* **29,** 2104, doi:10.1029/2002GL015434.
——, J. Oberhuber, A. Bacher, M. Esch, M. Latif, and E. Roeckner, 1999: Increased El Niño frequency in a climate model forced by future greenhouse warming. *Nature,* **398,** 694–696.
——, F.-F. Jin, and J. Abshagen, 2003: A nonlinear theory for El Niño bursting. *J. Atmos. Sci.,* **60,** 152–165.
Tudhope, A. W., and Coauthors, 2001: Variability in the El Niño–Southern Oscillation through a glacial–interglacial cycle. *Science,* **291,** 1511–1517.
Tziperman, E., L. Stone, M. Cane, and S. Zebiak, 1994: El Niño chaos: Overlapping of resonances between the seasonal cycle and the Pacific ocean–atmosphere oscillator. *Science,* **264,** 72–74.
Urban, F. E., J. E. Cole, and J. T. Overpack, 2000: Influence of mean climate change on climate variability from a 155-year tropical Pacific coral record. *Nature,* **407,** 989–993.
Vialard, J., C. Menkes, J.-P. Boulanger, P. Delecluse, E. Guilyardi, M. J. McPhaden, and G. Madec, 2001: A model study of oceanic mechanisms affecting equatorial Pacific sea surface temperature during the 1997–98 El Niño. *J. Phys. Oceanogr.,* **31,** 1649–1675.
Vossepoel, F. C., and D. W. Behringer, 2000: Impact of sea level assimilation on salinity variability in the western equatorial Pacific. *J. Phys. Oceanogr.,* **30,** 1706–1721.
Waliser, D. E., and N. E. Graham, 1993: Convective cloud systems and warm-pool SSTs: Coupled interactions and self-regulation. *J. Geophys. Res.,* **98,** 12 881–12 893.
Wallace, J., E. Rasmusson, T. Mitchell, V. Kousky, E. Sarachik, and H. von Storch, 1998: On the structure and evolution of ENSO-related climate variability in the tropical Pacific: Lesson. *J. Geophys. Res.,* **103,** 14 241–14 259.
Wang, B., and S.-I. An, 2001: Why the properties of El Niño changed during the late 1970s. *Geophys. Res. Lett.,* **28,** 3709–3712.
——, and ——, 2002: A mechanism for decadal changes of ENSO behavior: Roles of background wind changes. *Climate Dyn.,* **18,** 475–486.
Wang, C., 2001: A unified oscillator mode for the El Niño–Southern Oscillation. *J. Climate,* **14,** 98–115.
Wang, W., and M. J. McPhaden, 2000: The surface-layer heat balance in the equatorial Pacific Ocean. Part II: Interannual variability. *J. Phys. Oceanogr.,* **30,** 2989–3008.
White, H. G., 1980: Skewness, kurtosis and extreme values of Northern Hemisphere geopotential heights. *Mon. Wea. Rev.,* **108,** 1446–1455.
Wyrtki, K., 1985: Water displacements in the Pacific and the genesis of El Niño cycles. *J. Geophys. Res.,* **90C,** 7129–7132.
Xie, S. P., H. Annamalai, F. A. Schott, and J. P. McCreary, 2002: Structure and mechanisms of South Indian Ocean climate variability. *J. Climate,* **15,** 864–878.
Yu, X., and M. J. McPhaden, 1999: Dynamical analysis of seasonal and interannual variability in the equatorial Pacific. *J. Phys. Oceanogr.,* **29,** 2350–2369.
Zebiak, S. E., and M. Cane, 1987: A model El Niño/Southern Oscillation. *Mon. Wea. Rev.,* **115,** 2262–2278.